

# Optimised Graph Convolution for Calorimetry Event Classification

Matthieu Melennec<sup>\*1</sup>, Shamik Ghosh<sup>†1</sup>, and Frédéric Magniette<sup>‡1</sup>

<sup>1</sup> Laboratoire Leprince-Ringuet, École polytechnique - CNRS, Institut Polytechnique de Paris, Palaiseau, France

## Abstract

In the recent years, high energy physics discoveries have been driven by the increasing of luminosity and/or detector granularity. This evolution gives access to bigger statistics and data samples, but can make it hard to process results with current methods and algorithms. Graph convolution networks, have been shown to be powerful tools to address these challenges. We present our graph convolution framework for particle identification and energy regression in high granularity calorimeters. In particular, we introduce our algorithm for optimised graph construction in resource constrained environments. We also introduce our implementation of graph convolution and pooling layers. We observe satisfying accuracies, and discuss possible application to other high granularity particle detector challenges.

## 1 Introduction

The increase in luminosity at HL-LHC [1] and detector granularity for the CMS HGCAL upgrade [2] will allow to observe complex phenomena at an increased level of precision. This will increase the available statistics and precision by multiple orders of magnitude, which facilitates the detection of rare events, at the price of a significant increase of the number of channels. The challenge is that most of the standard techniques for reconstruction and triggering are not operative in such a context. For example, the energy threshold-based triggers fail to handle the complexity of high pile-up collisions. Neural network methods are known to handle noisy and complex data inputs well, and to deliver high level classification and regression. In particular, convolution techniques [3] have allowed outstanding improvement in computer vision. Unfortunately, they do not cope with the very peculiar topologies of particle detectors and the irregular distribution of their sensors. Alternatives such as spatial graph convolution have been developed to obtain the same classification power in that kind of non-euclidean environment [4]. It applies adapted convolution kernels to data represented as undirected graphs labelled by sensor measurements. These techniques have proven to give excellent results on the particle detector data at LHC [5] but also for neutrinos experiments [6]. They allow particle identification and continuous parameter regression, but also segmentation of entangled data which is a typical concern for overlapping particle showers.

We present the use of graph convolution neural networks for calorimeter object identification and energy regression, in the context of the OGCID project <sup>1</sup> (Optimisation of Graph Convolution for particle IDentification). In particular, we use the knowledge of the detector geometry to pre-compute proximities of potential node positions in the data to optimise the graph construction procedure, and discuss its time complexity. We also present the chosen message passing convolution operation, as well as introduce our pooling algorithm, Treclus, to coarsen local substructures, while preserving the overall structure of the graph. We present the graph readout pooling operation, used to flatten the outputs of convolution to an MLP of constant size. Finally, we present the classification and energy regression capacities of our pipeline, looking in particular at the resolution in energy to check the validity of our approach.

---

<sup>\*</sup>[matthieu.melennec@lfr.in2p3.fr](mailto:matthieu.melennec@lfr.in2p3.fr)

<sup>†</sup>[shamik.ghosh@lfr.in2p3.fr](mailto:shamik.ghosh@lfr.in2p3.fr)

<sup>‡</sup>[frederic.magniette@lfr.in2p3.fr](mailto:frederic.magniette@lfr.in2p3.fr)

<sup>1</sup><https://l1rogcid.in2p3.fr/>

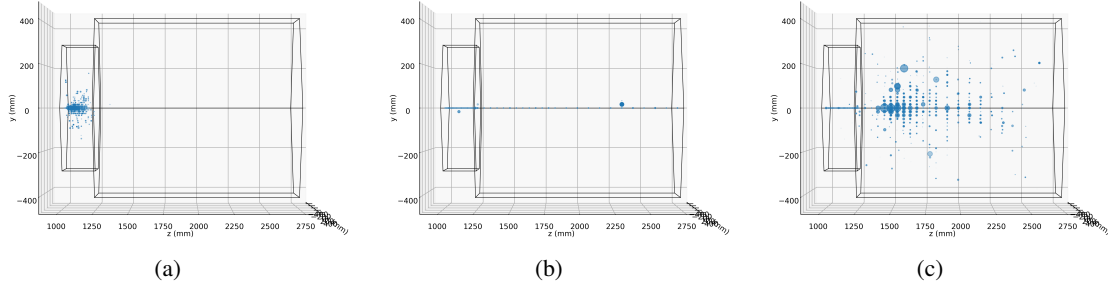


Figure 1: Event displays for (1a) an electron shower, (1b) a muon, (1c) a pion shower. Photon showers are very similar to electron showers [8].

## 2 The D2 Dataset

The data used in this study are extracted from the OGCID/D2 simulation dataset [7]. It is a set of single particle interaction with a simplified high granularity calorimeter inspired by CMS HGCAL [2].

This detector architecture features two main sections: the electromagnetic calorimeter (ECAL) and the hadronic calorimeter (HCAL), optimised for detecting particles of varying energies. The ECAL comprises 26 layers of lead absorbers (6.05 mm thick), while the HCAL has 24 layers of stainless steel absorbers, with 12 layers of 45 mm thickness and 12 of 80 mm, providing high resolution sampling of particle showers. Active silicon layers are placed between absorbers, segmented into hexagonal cells with a thickness of 0.32 mm and a transverse area of approximately  $1 \text{ cm}^2$  for ECAL and  $4 \text{ cm}^2$  for HCAL <sup>2</sup>.

The D2 dataset is a collection of simulated interactions between this detector and four types of particles (muon, positively charged pions, electrons and photons) at different energies and with a flat incidence angle (aligned with the longitudinal detector axis). The dataset includes detailed informations on each particle event, namely the energy measurement in each cell but also extracted variables of interest describing the geometry and the energy repartition of the hits.

For this study, we looked at electrons, photons, muons and pions with energies ranging from 10 to 100 GeV and aligned with the longitudinal axis. The event data that was used was the energy measurement in each cell.

## 3 Code Architecture

The pipeline used in this work is based on message passing convolution [9]. After generating graphs from the raw event data, these go through several layers of message passing convolution and pooling (CP layers). The resulting graphs are then flattened into a one-dimensional tensor by a readout pooling layer, which flattens the node features of the graphs in an orderly fashion. It also returns a structured tensor of constant size, independent of the input graph's size. This layer is essential to then feed the convoluted features to a multi-layer perception that will output our objective (particle ID or energy) by following a systematic pattern.

### 3.1 Graph Construction and Proximity Tables

Every calorimeter event is represented as a graph, the nodes of which correspond to every hit cell of the event, linked by arbitrarily defined edges. Our edge building strategy uses the  $k$  nearest neighbours (KNN) algorithm, to encode a sense of geometric locality in the graph structure. Our implementation of KNN is based off of so-called proximity tables (PTs), which contain a pre-computed order of neighbourhood for every sensor of the detector. That is, for every sensor of the detector, all other sensors are ordered according to a user-defined metric, as in Table 1. The graph building procedure then follows algorithm 1.

<sup>2</sup><https://llrogcid.in2p3.fr/hgcal-like-simulations/>

Sensor id	pos. 1	pos.2	...	$k$
1	$s_1^1$	$s_1^2$	...	$s_1^k$
2	$s_2^1$	$s_2^2$	...	$s_2^k$
$\vdots$	$\vdots$	$\vdots$	$\ddots$	$\vdots$
$i$	$s_i^1$	$s_i^2$	...	$s_i^k$

Table 1: Proximity table.  $s_i$  designates the sensor ID'd  $i$ ,  $s_i^k$  is the sensor in  $k$ -th position in the row for  $s_i$ . Letting  $m(s_i, s_i^k)$  be the value of the metric used to order the table, the neighbours of each sensors are ordered such that for any sensor  $s^i$  and any  $k$ ,  $m(s_i, s_i^k) \leq m(s_i, s_i^{k+1})$ .

---

**Algorithm 1** PTKNN: Proximity table  $k$  nearest neighbours graph generation algorithm.  $k$  is the number of neighbours wanted for each node.

---

```

1: Input: hits,  $k$ 
2: Output:  $G = \{V, E\}$ 
3:  $V \leftarrow \{\}$ 
4:  $E \leftarrow \{\}$ 
5: for  $s_i \in \text{hits}$  do
6:    $V \leftarrow V \cup \{s_i\}$ 
7:   counter  $\leftarrow 0$ 
8:   while counter  $< k$  do
9:     for  $s_i^k \in \{s_i^k\}_k$  do
10:    if  $s_i^k \in \text{hits}$  then
11:       $V \leftarrow V \cup \{s_i^k\}$ 
12:       $E \leftarrow E \cup \{(s_i, s_i^k)\}$ 
13:      counter  $\leftarrow$  counter + 1
14:    end if
15:  end for
16: end while
17: end for
18: return  $G = \{V, E\}$ 

```

---

Note that while it is standard to use the euclidean distance for the KNN algorithm, other metrics can be used to encode physical properties in the graph structure. For instance, one could use the correlation of cell hits as a metric, or connect the outermost nodes with the centre of the shower by introducing a radially term. In this study, the choice of the metric among the ones listed above and others derived from those seemed not to have an impact on the performance of the reconstruction. In the rest of this study, we therefore only use the simplest metric, which is the euclidean distance.

Intuitively, one understands that the PT-KNN algorithm brings an improvement to the KNN algorithm with regards to time complexity. Indeed, the KNN complexity is quadratic in both the worst case and on average. For the PT-KNN algorithm, while the worst case complexity can in theory increase to  $\mathcal{O}(NM)$ , with  $N$  the number of nodes and  $M$  the number of cells in the detector if  $M \gg N$ , this risk is mostly mitigated by the geometric locality of the shower (figure 1). In practice, in the range of number of nodes  $N$  corresponding to the size of a shower in the detector, the observed average last selected column  $\langle c_{\text{last}} \rangle$  gives an average complexity  $N \langle c_{\text{last}} \rangle \sim (\log N)^2$ . In the asymptotic range  $N \rightarrow \infty$  where  $N \gg (\log N)^2$ , one must consider the lower bound  $kN$  imposed by the PT-KNN algorithm, and we obtain a linear asymptotic complexity.

The value of  $\langle c_{\text{last}} \rangle$  is particularly relevant in the context of constrained computing, such as particle detector triggering algorithms. Indeed, reducing the size of the proximity table would greatly reduce the memory footprint of the PT. Hence knowing how far the PT is explored allows us to truncate the rows to  $\lambda \langle c_{\text{last}} \rangle$  columns for some  $\lambda$  to be determined. In practice, we observe that most often, the PT-KNN algorithm only explores 5% of the rows of the PT (figure 3). Hence a strong truncation of the depth of the PT would likely not have too big an impact on the graph structure while drastically reducing the size of the PT. The truncation of the proximity table also ensures that the worst case complexity reduces to  $\mathcal{O}(Nm_{\text{max}})$  with  $m_{\text{max}}$  the number of columns kept, with typically  $m_{\text{max}} \sim N$ .

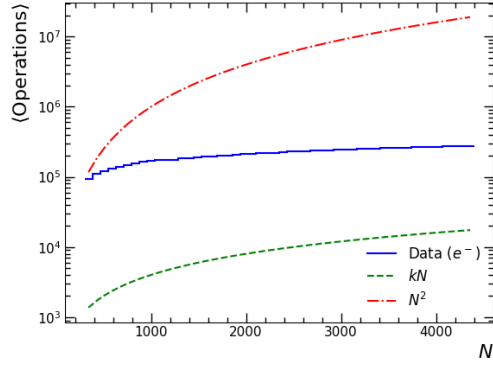


Figure 2: Average number of operations for the PT-KNN algorithm. A comparison shows linear and quadratic complexities. Asymptotically, the average number of operations behaves like  $O(kN)$

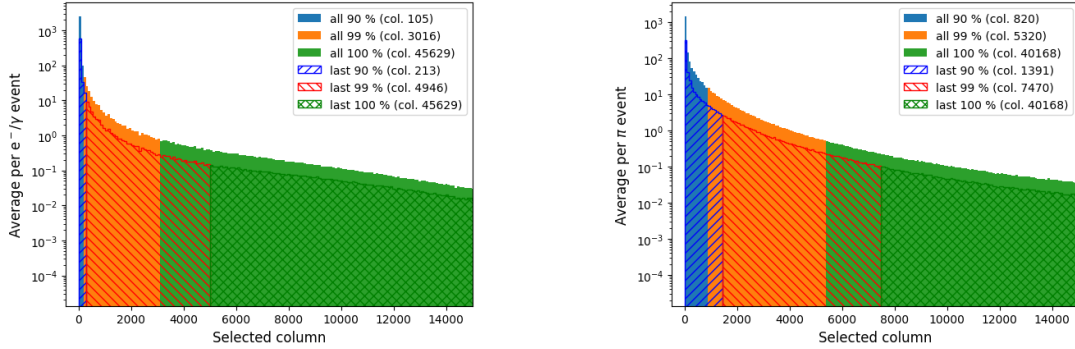


Figure 3: Column selections for PT-KNN algorithm with  $k = 4$ , euclidean distance at energies 10 to 100 GeV. We look at the columns of all selected neighbours (full areas) and at the last selected columns (hatched). We outline the  $x$ -th percentile of selected columns in either cases. We can benefit of the low variance of the distribution to impose strong cuts for a limited price on performance.

The resulting graphs are composed of nodes (or vertices)  $v \in V$ , holding as features the energy  $x_v$  measured by the corresponding sensor and the position  $\vec{u}_v$  of that sensor. Note that in order to respect the symmetries of shower formations in the detector, the position of the node is kept as a “hidden feature,” not used during the convolution operation. The positional information of the graph is encoded in the edges  $e_{vw} \in E$ , which carry as feature  $x_{vw} = \|\vec{u}_v - \vec{u}_w\|_2$  the euclidean distance between the end nodes  $v, w \in V$ , holding information about *relative* positions. In this study, we observed that the best trade-off between  $k$  and performance was reached for  $k = 4$ . All the graphs built in this work uses this value for  $k$ .

### 3.2 Message Passing Convolution

Message passing graph convolution can be seen as a generalisation of image convolution, were instead of operating on pixels, we operate on the nodes and/or edges of a graph. As for image convolutions, Message Passing Graph Convolution Neural Networks (MPGCNN) are built as successive layers of graph convolution and optional graph pooling, which we call CP layers. Since the edges of the graphs we look at have been built arbitrarily and only encode relative positions in their features, we only apply the convolution operation on nodes. The convolution operation for nodes is defined in [9] as follows: given a graph  $G = (V, E)$ , we denote the feature vectors of the nodes  $v \in V$  at CP layer  $l$  as  $x_v^{(l)}$  (note that  $x_v^{(0)}$  is the energy measured by the sensor associated to  $v$ ). At every convolution step of a layer, new features  $x_v^{(l+1)}$  are obtained from the old features  $x_v^{(l)}$  and  $x_w^{(l)}$  of  $v$  and its neighbours  $w \in \mathcal{N}(v)$ :

$$x_v^{(l+1)} = \gamma_{\theta_\gamma} \left( x_v^{(l)}, \square_{w \in \mathcal{N}(v)} \phi_{\theta_\phi} \left( x_v^{(l)}, x_w^{(l)}, x_{vw} \right) \right) \quad (1)$$

Here,  $\phi_{\theta_\phi}$  is the message function, combining the features of  $v$ , of a neighbour  $w \in \mathcal{N}(v)$  and the features  $x_{vw}$  of their linking edge  $e_{vw}$ . It is parametrised by learnable parameters  $\theta_\phi$ , and is usually implemented as a shallow MLP.  $\square$  is the aggregator, updating the current node’s features with the aggregated messages from neighbours. Since the number of neighbours of  $v$  may vary, the aggregation operator must be normalised and commutative. Typical aggregators are max or mean functions.  $\gamma_{\theta_\gamma}$  is the update function, mixing the aggregated messages and the node features. It is usually implemented as a shallow MLP, and has trainable parameters  $\theta_\gamma$ .

In our implementation, we chose the message function to be a single layer of neurons with a Leaky-ReLU activation function, taking as input  $\chi$ , the concatenated features  $x_v$ ,  $x_w$  and  $x_{vw}$ :

$$\begin{aligned} \phi_{\theta_\phi} (x_v, x_w, x_{vw}) &= \text{Leaky-ReLU} \left( \Theta_\phi \chi \right), \\ \chi &:= [x_v, x_w, x_{vw}] \in \mathbb{R}^{2n+m} \end{aligned} \quad (2)$$

where  $n$  denotes the number of features per node,  $m$  the number of features per edge, and  $\Theta_\phi \in \mathbb{R}^{l \times (2n+m)}$  is a matrix of trainable weights, with  $l$  the output size of the message function. The chosen aggregator  $\square$  depends on the task at hand. In the case of a particle ID problem, we take a feature-wise max pooling, to outline protruding features [10], while for regression we use mean pooling to smoothen protruding features and consider the graph globally [11, 12]. Finally, noting that the update function is a way to combine aggregated neighbour convoluted features with features  $x_v$ , we chose  $\gamma_{\theta_\gamma}$  to be the aggregation of the aggregated messages with the features of the node  $v$  itself. In practice, this is equivalent to adding self-loops to the graphs, i.e. for any  $v \in V, e_{vv} \in E$ .

$$\begin{aligned} &\gamma_{\theta_\gamma} \left( x_v^{(l)}, \square_{w \in \mathcal{N}(v)} \phi_{\theta_\phi} \left( x_v^{(l)}, x_w^{(l)}, x_{vw} \right) \right) \\ &= \phi_{\theta_\phi} (x_v, x_v, x_v) \square \left( \square_{w \in \mathcal{N}(v)} \phi_{\theta_\phi} (x_v, x_w, x_{vw}) \right) \\ &= \square_{w \in \tilde{\mathcal{N}}(v)} \phi_{\theta_\phi} (x_v, x_w, x_{vw}) \end{aligned} \quad (3)$$

with  $\tilde{\mathcal{N}}(v) = \mathcal{N}(v) \cup \{v\}$ . In our case, the edge features are the euclidean distance between nodes. As such, for any node  $v$ ,  $x_{vv} = 0$ .

### 3.3 Graph Pooling

Graph pooling is an important step in graph convolution, as it allows to coarsen the graph, hence looking at the graph on a more global scale [13]. First, let us express the steps of a graph pooling operation as in [14], with a clustering

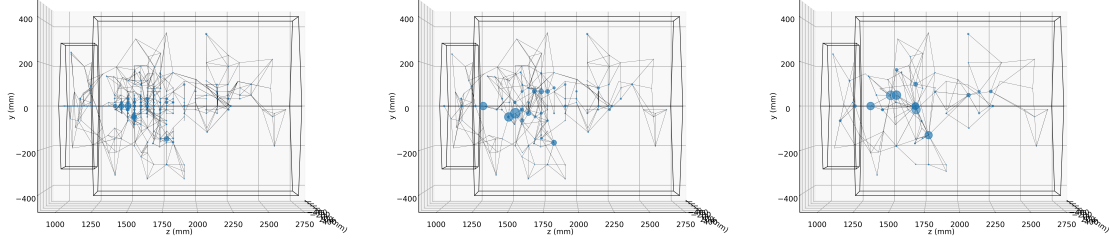


Figure 4:  $\pi^+$  shower graph representation after successive pooling steps. We indeed observe that while the number of nodes decreases, the global shape of the graph is preserved through pooling.

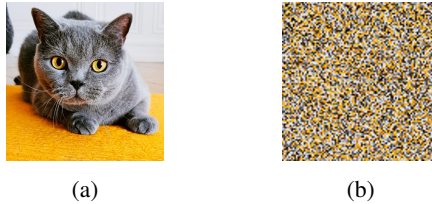


Figure 5: While an image with an expected and ordered structure (5a) is easily interpreted, a random order (5b) makes it uninterpretable.

step, where we select which nodes will be clustered together, followed by a reduction step, where nodes within clusters are pooled, and finally a connection step, during which we update the adjacency of clusters. In our case the graphs are embedded in a euclidean space, and we therefore want to cluster together neighbours that are geometrically close to one another, as illustrated in figure 4. To this end, we developed a threshold clustering algorithm, called Treclus, that creates a matching of the graph [15], where matched nodes are linked by an edge shorter than a threshold  $\varepsilon$ , and clusters matched nodes together. It is very important that the clustering edges make a matching to keep a linear complexity of the clustering algorithm. This however implies that clusters may only contain two nodes, while we ideally wish to find a maximum matching of the subgraph  $G' = (V, E' = \{e \in E | e \leq \varepsilon\})$ , which is usually a quadratic problem [16]. Our approach therefore consists in applying the Treclus algorithm multiple times in a row to increase the number of clustered short edges with limited impact on complexity. We observed that less than 10 calls to Treclus suffice to collapse all edges shorter than the 30-th percentile of edges after at most 2 CP layers. The choice of the 30-th percentile was done to match the number of clusters resulting from the clustering process with the factor of increase of features during the convolution to ensure all information is conserved without redundancy.

The reduction step consists of a feature wise pooling of nodes within the same clusters. The choice of the pooling operation follows the same logic as the aggregator function choice for the convolution step. However, while this applies strictly for the classification task (with a max pooling), for the energy regression step, the aggregator must be a feature-wise sum to conserve information about the number of nodes contained in the cluster. The position of the cluster is taken at random from one of the nodes it contains. This allows to keep the graph embedded in the known detector geometry (see section 3.4) while preserving the locality of the cluster, since the length of the remaining edges makes the induced error negligible. The random choice in position however imposes an upper-bound on the threshold  $\varepsilon$ , which in turn limits the output size of the convolution operation to avoid overfitting, reducing the size of the network.

Finally, for the reconnection step, the clusters inherit their adjacencies from their nodes, i.e. two clusters are neighbours if they each contain neighbouring nodes. The length of these edges is then re-computed to smoothen the accumulation of errors due to the random choice of cluster positions.

### 3.4 Graph Readout Pooling

After the convolution and pooling layers, it is necessary to flatten the graph representation if the output of convolution needs to be fed into a multi-layer perceptron (MLP). This operation, known as readout (or readout pooling), can be quite tricky, as graph-like data usually does not have any consistent ordering and may have variable sizes. The importance of ordering for the readout operation is illustrated in figure 5. The same applies to the readout of graphs and the ordering of nodes [17]. Our approach uses the fact that we know the detector geometry, and kept the nodes

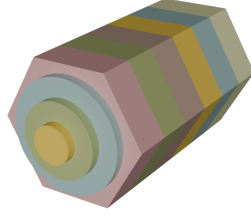


Figure 6: Radial readout regions of the detector. Each longitudinal slice of the detector is divided in concentric cylindrical regions, respecting radial symmetry. The design of the readout regions respects the rotational symmetry of the detector.

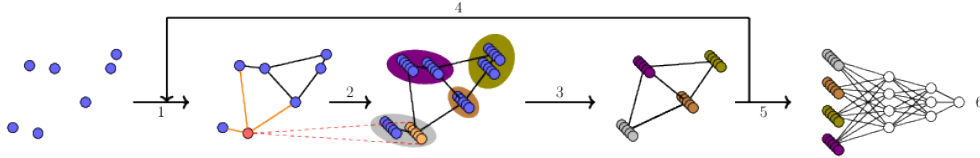


Figure 7: Typical message passing GNN pipeline. (1) Graph generation (2) Message passing convolution - Nodes collect “messages” from their neighbours (3) Pooling (4) Repeat CP layers (5) Readout (6) Objective (PID or Energy regression)

embedded (through the hidden features) in that geometry (see “reduction” paragraph of Sec. 3.3) to re-embed the graph back into the detector, and divide the detector into different *readout regions*. Using the same argument and procedure as in section 3.3, all nodes within the same readout region are feature-wise pooled together, and the obtained feature of every region are flattened following a known order. It is however important that this voxelisation of the detector respects the geometry of the detector. Indeed, the HGCAL model that we considered in this study has a rotational symmetry. If we rotated an electron shower in the detector, while it is the same input, if the readout does not respect that symmetry in the detector (see figure 6) the model would have to learn both showers as two different inputs with identical output. This would hinder the training time and performance greatly. Note that the detector being composed of two different types of detector, electromagnetic and hadronic calorimeters, we can adapt the granularity of the readout to the task at hand: in energy regression tasks for electrons or photons, where there is no interaction with the hadronic part of the detector, a higher granularity of the readout is only needed in the ECAL.

### 3.5 Single Particle Reconstruction Pipeline

All the elements presented above allow us to design a pipeline for the reconstruction (particle ID and energy regression) of calorimeter events. The pipeline aims at identifying the detected particle and regressing its energy. The workflow is illustrated in figure 8. The first step is to generate graphs from raw detector data, using the PT-KNN algorithm. A first pipeline is trained for particle classification. Because electromagnetic and hadronic showers have very different signatures in the detector, there are two energy regression GNNs, for either of these signatures. In the case of muons, their energy when passing through the detector is in the minimum ionisation range [18], making it very hard to regress their energy, especially without a magnetic field, as is the case in this simulation. All pipelines have the same structure of repeated convolution and pooling layers, followed by a readout layer for the input of an MLP. Their exact definition slightly differ, most importantly by the choice of threshold for Treclus, either dataset specific or generalist (all particles

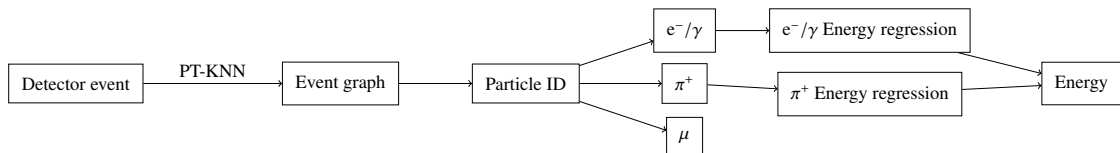


Figure 8: Algorithmic workflow of the single particle full reconstruction pipeline



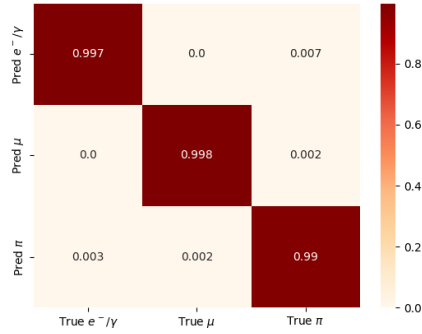


Table 2: Confusion matrix of the particle classifier pipeline. Each entry is the fraction of particles that were identified as the corresponding prediction. Entries are normalised within each true class of particles.

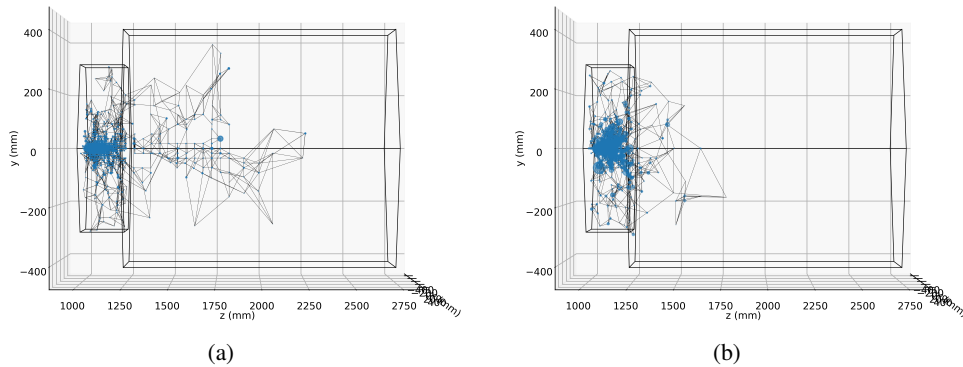


Figure 9: Example misclassified events. They have the typical signatures of the particles they are misidentified as. (9a) An electron induced hadronic shower (9b) An early showering pion.

at once), and in the granularity of the readout, chosen to be maximal in the regions of interest (whole detector, ECAL or HCAL) while not imposing an MLP size that would be too big. For all GNN pipelines, we apply 3 layers of convolution and pooling. At every CP layer, the number of node features doubles while the number of nodes is divided by two. For readout, the granularities depend on the task at hand. For the particle ID, we need a granular readout for the full detector, both longitudinally (for  $e^-/\gamma$  and  $\pi^+$  classification) and radially (to distinguish  $\mu$ , which do not spread radially in the detector). As such the ECAL is divided in 3 concentric region, while the HCAL has 4 longitudinal regions, divided in respectively 3, 3, 2 and 2 concentric regions. For energy regression tasks, we divide the concerned part of the detector (ECAL or HCAL) with a granular readout (3 to 6 longitudinal slices, dependent on the length of the region, divided each in 3 concentric cylinders), while keeping the rest of the detector as a single readout region. Finally, the MLP is funnel-shaped comprised of 6 layers with leaky ReLU activation.

## 4 Results

### 4.1 Particle Identification

We first look at the classifying performance of the GNN pipeline presented above. As can be guessed from Figure 1, this is mostly a density problem and the choice of readout regions is the key element of this task. From the confusion matrix (table 2) we can see a good classification performance. If we look at the raw detector output of misclassified elements (figure 9), we observe that most errors are due to outlier events, such as electromagnetic showers leaking into the HCAL, electron induced hadrons, later detected in the HCAL or early showering pions.



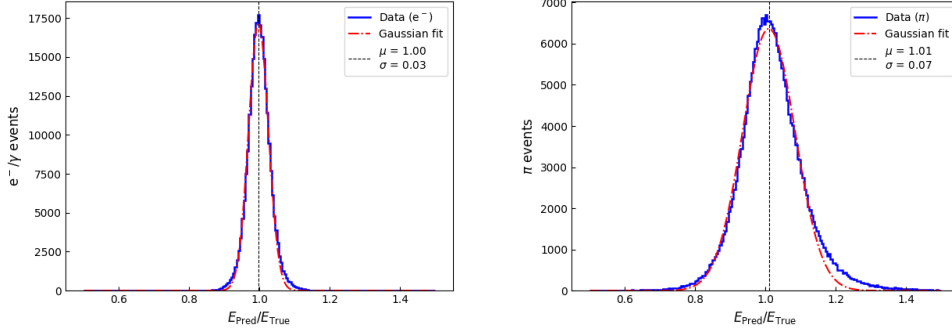


Figure 10: Energy response  $E_{\text{pred}}/E_{\text{true}}$ . We observe gaussian-like distributions centred at 1. Electromagnetic showers have a smaller standard deviation than for pions. This is due to the difference in sampling fractions in the ECAL and HCAL, as well as the nature of the showers.

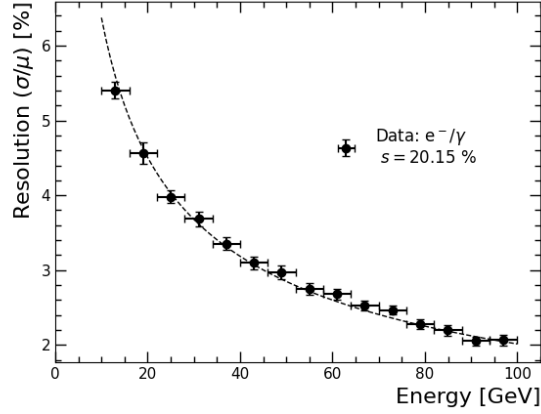


Figure 11: Electron energy resolution in the detector. We recover a stochastic term of  $S_{\text{GNN}} = 20.15\% \sim S_{\text{exp}}$

## 4.2 Energy Regression

The training of the energy regression pipelines was done with events classified by the Particle ID pipeline as either  $e^-/\gamma$  or  $\pi^+$ . We define the response as the ratio  $E_{\text{pred}}/E_{\text{true}}$  and use it as a metric for performance. We observe a Gaussian-like distribution centred around 1 (see figure 10). We also look at the energy resolution

$$\left( \frac{\sigma\left(\frac{E_{\text{pred}}}{E_{\text{true}}}\right)}{\left\langle \frac{E_{\text{pred}}}{E_{\text{true}}}\right\rangle} \right)^2 = \left( \frac{S}{\sqrt{E_{\text{true}}}} \right)^2 + \left( \frac{N}{E_{\text{true}}} \right)^2 + C^2 \quad (4)$$

with  $S$  the stochastic term, describing the physical fluctuations in shower development,  $N$  the noise term, describing the electronic noise from the detector readout electronics and  $C$  the constant term, describing systematic noise [19]. Note that in our simulation, no readout or systematic noise have been emulated. We therefore only consider  $\frac{\sigma}{\mu} \propto \frac{1}{\sqrt{E}}$ , as seen in figure 11. For the electromagnetic calorimeter, we find a stochastic term  $S_{\text{GNN}} = 20.15\%$ , close to the theoretical value  $S_{\text{exp}}$  of 20%.

## 5 Conclusion

### 5.1 Outlook

Our framework, by its generic and detector agnostic nature, can be generalised to other problems in high granularity particle detectors with a non-regular architecture. Examples of other problems to which it could be used include neutron capture detection and vertex reconstruction in the IBD detection channel for diffuse supernova neutrino background searches in Super and Hyper-Kamiokande [20] or overlapping object segmentation in granular detectors (HGAL or Hyper-Kamiokande like).

### 5.2 Summary

We presented a message passing graph convolution neural network architecture for particle identification and energy regression in high granularity calorimeters. We introduced the use of Proximity Tables and the PT-KNN algorithm for optimised graph construction. In particular, we discussed the improved average time complexity compared to the classical KNN algorithm. We also discussed the possibility to reduce the size of proximity tables for PT-KNN implementation in resource constrained environments such as on FPGAs. We also presented our implementation of message passing convolution and pooling layers. Treclus, our threshold based clustering algorithm for geometric pooling of graph has proven to be very adapted to coarsen graphs while preserving the original global structure of the graph. We discussed the need for a graph readout pooling to feed the result of the convolution layers to an MLP. We implemented a segmentation of the detector based on the geometry of the physical processes at hand to flatten the graph structure in a fixed size tensor while preserving the symmetries of the problem. Finally, we discussed the state of the art level classification and energy regression capacities of our GNN implementation. Looking at the energy resolution of our algorithm, we recover the expected values, proving the validity of our approach.

## 6 Acknowledgements

We are grateful for the Agence Nationale de la Recherche, financing the OGCID project under funding ANR-21-CE31-0030.

## References

- [1] I. Zurbano Fernandez *et al.*, “High-Luminosity Large Hadron Collider (HL-LHC): Technical design report,” vol. 10/2020, 12 2020.
- [2] C. collaboration, “The Phase-2 Upgrade of the CMS Endcap Calorimeter,” tech. rep., CERN, Geneva, 2017.
- [3] Z. Li, F. Liu, W. Yang, S. Peng, and J. Zhou, “A survey of convolutional neural networks: Analysis, applications, and prospects,” *IEEE Transactions on Neural Networks and Learning Systems*, vol. PP, pp. 1–21, 06 2021.
- [4] Z. Zhang, P. Cui, and W. Zhu, “Deep learning on graphs: A survey,” *IEEE Transactions on Knowledge and Data Engineering*, vol. 34, pp. 249–270, jan 2022.
- [5] S. R. Qasim, J. Kieseler, Y. Iiyama, and M. Pierini, “Learning representations of irregular particle-detector geometry with distance-weighted graph networks,” *The European Physical Journal C*, vol. 79, July 2019.
- [6] N. Choma, F. Monti, L. Gerhardt, T. Palczewski, Z. Ronaghi, P. Prabhat, W. Bhimji, M. M. Bronstein, S. R. Klein, and J. Bruna, “Graph neural networks for icecube signal classification,” in *2018 17th IEEE International Conference on Machine Learning and Applications (ICMLA)*, pp. 386–391, 2018.
- [7] E. Becheva, F. Beaudette, J.-B. Sauvan, M. Melennec, S. Ghosh, M. Mellin, and F. Magniette, “High granularity calorimetry d2 dataset.” <https://zenodo.org/records/14260279>.
- [8] R. Wigmans, *Calorimetry: Energy Measurement in Particle Physics*. International series of monographs on physics, Oxford University Press, 2017.

- [9] J. Gilmer, S. S. Schoenholz, P. F. Riley, O. Vinyals, and G. E. Dahl, “Neural message passing for quantum chemistry,” in *Proceedings of the 34th International Conference on Machine Learning - Volume 70*, ICML’17, p. 1263–1272, JMLR.org, 2017.
- [10] I. Goodfellow, Y. Bengio, and A. Courville, *Deep Learning*. MIT Press, 2016. <http://www.deeplearningbook.org>.
- [11] G. Huang, Z. Liu, L. Van Der Maaten, and K. Q. Weinberger, “Densely connected convolutional networks,” in *2017 IEEE Conference on Computer Vision and Pattern Recognition (CVPR)*, pp. 2261–2269, 2017.
- [12] F. N. Iandola, M. W. Moskewicz, S. Karayev, R. B. Girshick, T. Darrell, and K. Keutzer, “Densenet: Implementing efficient convnet descriptor pyramids,” *ArXiv*, vol. abs/1404.1869, 2014.
- [13] M. Defferrard, X. Bresson, and P. Vandergheynst, “Convolutional neural networks on graphs with fast localized spectral filtering,” in *Advances in Neural Information Processing Systems* (D. Lee, M. Sugiyama, U. Luxburg, I. Guyon, and R. Garnett, eds.), vol. 29, Curran Associates, Inc., 2016.
- [14] D. Grattarola, D. Zambon, F. M. Bianchi, and C. Alippi, “Understanding pooling in graph neural networks,” *IEEE Transactions on Neural Networks and Learning Systems*, vol. 35, no. 2, pp. 2708–2718, 2024.
- [15] L. Lovász and M. Plummer, *Matching Theory*. AMS Chelsea Publishing Series, AMS Chelsea Pub., 2009.
- [16] S. Behnezhad, M. Roghani, and A. Rubinstein, “Approximating maximum matching requires almost quadratic time,” in *Proceedings of the 56th Annual ACM Symposium on Theory of Computing*, STOC 2024, (New York, NY, USA), p. 444–454, Association for Computing Machinery, 2024.
- [17] M. Zhang, Z. Cui, M. Neumann, and Y. Chen, “An end-to-end deep learning architecture for graph classification,” vol. 32, Apr. 2018.
- [18] R. L. Workman *et al.*, “Review of particle physics,” *PTEP*, vol. 2022, p. 083C01, 2022.
- [19] C. W. Fabjan and F. Gianotti, “Calorimetry for particle physics,” *Rev. Mod. Phys.*, vol. 75, pp. 1243–1286, Oct 2003.
- [20] J. F. Beacom and M. R. Vagins, “Antineutrino spectroscopy with large water Čerenkov detectors,” *Phys. Rev. Lett.*, vol. 93, p. 171101, Oct 2004.